Ultra-Reliable and Low-Latency Vehicular Communication using Optical Camera Communications

Amirul Islam, Leila Musavian, and Nikolaos Thomos

Abstract

Optical camera communication (OCC) has emerged as a key enabling technology for the seamless operation of future autonomous vehicles. By leveraging the supreme performance, OCC has become a promising solution to meet the stringent requirements of vehicular communication to support ultra-reliable and low-latency communication (uRLLC). In this paper, we introduce a novel approach of capacity maximization in vehicular OCC through the optimization of capacity, power allocation, and adaptive modulation schemes while guaranteeing reliability and latency requirements. First, we formulate a vehicular OCC model to analyze the performance in terms of bit-error-rate (BER), achievable spectral efficiency, and observed latency. We thus characterize reliability over satisfying a target BER, while latency is determined by considering transmission latency. Then, a capacity maximization problem is formulated subject to transmit power and uRLLC constraints. Finally, utilizing the Lagrange formulation and water-filling algorithm, an optimization scheme is proposed to find the adaptive solution. To demonstrate the robustness of the proposed optimization scheme, we translate the continuous problem into a discrete problem. We justify our proposed model and optimization formulation through numerous simulations by comparing capacity, latency, and transmit power. Simulation results show virtually no loss of performance through discretization of the problem while ensuring uRLLC requirements.

Index Terms

Ultra-reliable and low-latency communication (uRLLC), vehicular communication, optical camera communication (OCC), capacity maximization.

A. Islam, L. Musavian, and N. Thomos are with the School of Computer Science and Electronic Engineering, University of Essex, UK (e-mail: amirul.islam@essex.ac.uk; leila.musavian@essex.ac.uk; nthomos@essex.ac.uk).

I. INTRODUCTION

Driven by vehicular networks, the automotive industry is undergoing key technological transformations through automotive vehicles (AV). In the modern world, the number of vehicles and vehicle-assisting infrastructures are increasing rapidly, making the transportation system more vulnerable than ever, resulting in more traffic congestions, road causalities, and overall less road safety. These rapid growths of the number of vehicles will open a significantly challenging, but profitable market, for the future intelligent transportation system (ITS) [1]. To cope with the current evergrowing and complex vehicular networks, the practice of sharing information and cooperative driving on the road is substantially increasing. However, the deployment of communications between AVs can help to ensure traffic safety and enhance the overall driving experience by facilitating new services, such as collision avoidance and autonomous driving [2], [3]. Though several vehicle-to-vehicle (V2V) applications, such as lane changing alert, automotive braking system, have already been deployed, mission-critical services, e.g., collision avoidance, automotive driving, and other safety-related issues, are still creating severe challenges. Therefore, providing efficient V2V communications is necessary for enabling future ITS [4]. The performance of the growing transportation systems depends on the availability of V2V communication links at ultra-low latency and errors. As a result, data should be delivered within a short time, providing a high probability of success.

However, achieving the required latency and reliability concurrently makes the V2V communication more challenging. For enabling uRLLC in ITSs, several methods, such as [5]–[9], reflect on delay minimization, reliability guarantee, vehicle clustering, and excess queue length evaluation. Specifically, in [5], the vehicular network transmission power is minimized by grouping vehicles into clusters and modelling reliability as queuing delay violation probability. In [6], a joint resource allocation and power control algorithm is proposed to maximize the V2V rate considering latency and reliability constraints. In [7], the authors study the impact of transmission time interval on the performance of low-latency vehicular communications. Considering the ultra-reliable communication perspective, average rate maximization was evaluated using signal-to-interference ratio coverage in [8]. Recently, several principles of uRLLC are surveyed in [9]. Moreover, edge computing is also considered as an attractive solution to minimize latency that processes the requested tasks locally, without relying on remote servers [10], [11].

The above-mentioned methods enable uRLLC, either using radio frequency (RF) or cellular-

TABLE I

COMPARISON BETWEEN OCC, PD, AND RF

Parameter	OWC		RF
	OCC	PD	
Bandwidth of carrier	Unlimited (400 - 700) nm	Unlimited (400 - 700) nm	300 GHz (saturated and regulated)
EMI and hazard	No	No	Yes
Transmitter	LED	LED or Laser diode (LD)	Antenna
Receiver	Camera	PD	Antenna
Power consumption	Relatively low	Relatively higher than OCC	Medium
Interference level	Negligible	Low	Very high
Distance covered	200 m	10 m	More than 100 km
Environmental effect	No	Indoor: No, Outdoor: Yes	Yes
Noise	No	Sun and ambient light sources	Electrical and electronic devices
Security	High	High	Low
Data rate	54 Mbps	10 Gbps using LED and 100 Gbps using LD	6 Gbps (IEEE 802.11ad at 60GHz)
Main purpose	Illumination, communication, and localization	Illumination and communication	Communication and positioning
Limitation	Low data rate	Short distance, no mobility guaranty, and unsuitable for outdoor	Interferences

based communication systems with central base stations (BS), remote or edge servers, mostly relying on centralized resource management. However, these servers have limited computational resources, and therefore, they can easily be overloaded with the frequently requested AV tasks. Moreover, if it is coupled with complex and randomly varying channels, optimizing uRLLC will be very challenging, and it may require faster and efficient distributed algorithms. Most importantly, the security can be violated as information are exchanged between the servers and vehicles or infrastructures during communication and decision making. Besides, RF channels are prone to channel fading, noise, or interference.

On the contrary, recently, visible light communications (VLC) have attracted tremendous attention as next-generation communication services [12], [13] that can be alternative to RF. VLC uses LEDs as transmitter and camera or photodiode (PD) as the receiver. VLC offers various advantages over RF system, for example, a license-free unlimited spectrum, longer lifespans, lower implementation cost, and enhanced security for having the line-of-sight (LOS) properties [14]. It does not harm human bodies or eyes and is not affected by electromagnetic interference

(EMI). Furthermore, VLC is easier to integrate with the existing vehicular systems at the lowest cost without any significant infrastructure changes because LED lights are already existing in vehicles, traffic lights or infrastructures. VLC system employing cameras as the receiver is known as OCC, whereas those use PD are called light-fidelity. PDs are generally small non-imaging devices, which produce a quick response. But, it offers restrictions due to the trade-off between transmission range and signal reception. The use of cameras mitigates the challenges in PD.

Table I summarizes the comparison between OCC, PD, and RF-based systems, which shows that OCC suffers nearly negligible interference and consumes less power than RF. Besides, OCC supports almost 20 times longer distance than the PD-based systems. Although having low data rate, OCC can be a better alternative to the congested and saturated RF system due to its negligible noise and interference and higher security. OCC can spatially separate and process different transmitter sources independently on its image plane [15], which enables interference-free communication. However, OCC can face challenges due to its LOS requirements for communication.

Besides OCC, vehicular ad-hoc networks (VANETs) created immense opportunities in the ITS at lower operational cost [16], [17]. But, VANETs have shortcomings, such as lower accuracy, unreliable Internet service, and lack of pure network architecture [18]. Alternately, AV communication uses wireless access in vehicular environments, i.e., IEEE 802.11p standard [19]. But OCC suppresses IEEE 802.11p with advantages of the unlicensed and huge frequency spectrum, BS independency, and simultaneous lighting, localization, and communication functionalities. The revolutionary advancements and potential advantages of OCC have led the technology as a promising mechanism for the future AV communication [15], [20], [21]. Several vehicular OCC systems are trying to improve the BER and capacity performances. However, none of them tried to address uRLLC challenges until now.

In our previous paper [22], we analyzed the performance of vehicular OCC to justify whether OCC will be suitable for satisfying uRLLC in AVs. In this current paper, we propose a new scheme of guaranteeing uRLLC requirements in vehicular OCC by maximizing expected capacity through adaptive power allocation and adaptive adjustment of a specified discrete modulation set. The system will develop a fully decentralized communication scheme, where each vehicle will individually process the received surrounding information from different vehicles. Moreover, our proposed system guarantees higher security, as OCC employs LOS communication and decentralized information processing. In our evaluation, BER is used to characterize the reliability

requirement, and transmission latency is considered to define the end-to-end (E2E) latency. We neglect computational latency as a small amount of data (related to the action or safety information) is managed in our system. As our goal is to avoid the critical condition, i.e., avoid collision between vehicles, thus satisfying uRLLC between V2V links is needed to operate the vehicles effectively. To improve the efficiency of vehicular OCC, we use an adaptive modulation scheme because higher spectral efficiency and lower latency can be achieved by increasing the modulation order. Therefore, this paper investigates the problem of capacity maximization and transmit power allocation, as well as adaptive adjustment of modulation scheme for vehicular OCC, which guarantees the E2E latency and reliability requirements of V2V communication. The main objective of the proposed scheme is to maximize the expected rate among the V2V links subject to the latency and BER requirements as well as average transmit power constraint. The major contributions of this paper are summarized as follows:

- We mathematically model the vehicular OCC channel in order to analyze the performance of the probability of errors, achievable spectral efficiency, and transmission latency at different inter-vehicular distances and AoIs while considering the adaptive modulation.
- The capacity maximization problem is formulated for vehicular OCC system considering transmit power allocation. We then transform the continuous capacity optimization problem into a discrete capacity problem subject to average transmit power, BER, latency, and adaptive modulation scheme constraints. We mathematically prove that the former problem (continuous) is concave with respect to transmit power, which hence, can be solved using Lagrange relaxation method. A water-filling algorithm is used to allocate the average transmit power effectively.
- We investigate the effect of the proposed algorithm on the performance of capacity, latency, and transmit power while satisfying uRLLC requirements, which shows that the proposed method offers approximately identical results for both discrete and continuous problems, even after transformation into the discrete rate.

The remainder of this paper is organized as follows. Section II outlines the vehicular OCC channel model and mathematical representation of the performance parameters of the proposed V2V system. Section III proposes the formulation of capacity maximization problem subject to the reliability and latency constraints. The solution to the optimization problem is presented in IV. Section V describes the simulation results with details description of simulation methods

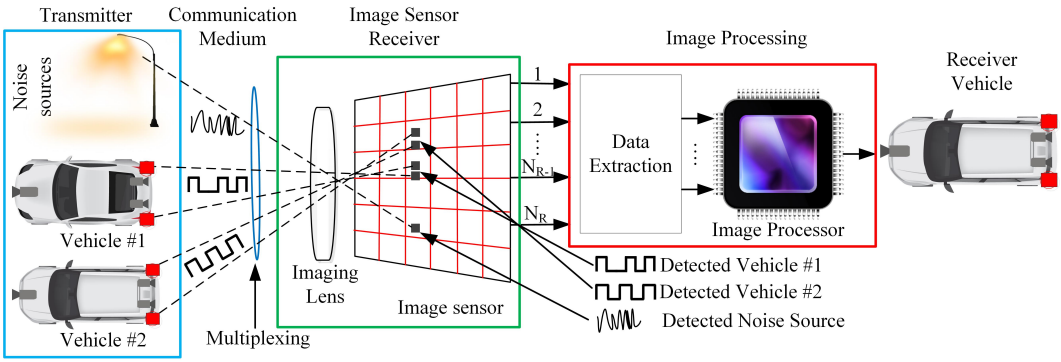

Fig. 1. An illustration of vehicular optical camera communication operation.

and parameters. Finally, our conclusions are offered in Section VI.

II. System Model of Vehicular OCC

In this section, we present the system model with the performance analysis of vehicular OCC. We start by presenting the overview and the state of the art of vehicular OCC. Then, the modelling of the proposed scenario and the definitions of the model parameters are explained. Finally, we model the performance defining parameters of OCC in terms of the BER, the spectral efficiency, the achievable channel capacity, and the observed E2E latency. [1]

A. Overview of Vehicular OCC

OCC is a promising technology with the benefit of line-of-sight (LOS) and illumination functionality and its considerable superiority over existing communication technologies, e.g., radio waves or PD-based communication [20], [23]. In general OCC architecture, LED arrays located on the rear side of a vehicle or other light (noise) sources act as transmitters, and cameras act as the receiver (see Fig. 1). The LED arrays transmit vehicular safety information, including traffic information, LED coordinates, and vehicle's internal information, e.g., speed, next move, and position. Meanwhile, the camera at the receiver vehicle captures the video frames of the LED arrays, which pass through an imaging lens. From the captured images, the image processor decodes signal information using a suitable demodulation technique, which is updated to the processing unit of the system. Finally, the receiver vehicle performs particular actions, e.g., reduce speed, change directions, and place brakes, based on the decoded information.

[1] In this paper, we use the terms image sensor and camera interchangeably.

In recent years, there have been notable advancements in the application of cameras for various services, such as multimedia, broadcasting, localization, and ITS [15], [24]. Cameras capture image pixels from the observed scenes within their field-of-view (FoV) that are projected from various light sources. In vehicular OCC, no complex signal processing algorithm is required to filter out the light sources that convey no information. These can be completely discarded by the camera. As shown in Fig. 1, two transmitters (Vehicle #1 and Vehicle #2 -LED arrays) transmit communication information through LED lights, and other light sources, e.g., Sunlight, ambient lights, traffic lights, and digital signages, are considered as noise sources. These noise and data sources can easily be captured and distinguished distinctively on the image plane of the image sensor, and the pixels associated with noise sources can be separated and discarded easily as cameras only focus on the pixels in which the LED lights strike. In this manner, interference-free and secure communications can be achieved using an image sensor.

Though several vehicular systems based on global positioning system (GPS), light detection and ranging (LiDAR) are implemented for vehicular positioning or ranging applications [25]; but GPS is not a reliable positioning technique in the vehicular environment due to the inaccuracy in precise positioning. On the other hand, the LiDAR system does not include any communication mechanism with the surrounding vehicles or infrastructures, while its implementation is very costly and requires a more complicated system. But, the information of the surrounding vehicles or infrastructures is the most significant factor for future AVs and ITS, and this is why various studies of the capabilities, potentials, and advantages of the OCC system have already been conducted. Based on the LED lights intensity variation, a flag image was generated via communicated image pixels, which achieved 10 Mbps data rate [21]. In [26], the data rate was improved to 15 Mbps with 16.6 ms real-time LED detection and classification. In [14], the transmission rate was improved to 54 Mbps with BER $< 10^{-5}$ and to 45 Mbps with zero BER at 50 m distance.

However, the above mentioned schemes tried to enhance performance by improving the data rate with experimental analysis, but none of them have considered the resource allocation or uRLLC performance analysis under the consideration of interferences for vehicular OCC. In this paper, we propose a novel capacity maximization technique for satisfying uRLLC requirements through performance analysis of vehicular OCC. To the best of our knowledge, this is the first time where uRLLC is analyzed and optimized in vehicular OCC. In the following sub-sections, the proposed system model is explained together with the performance analysis.

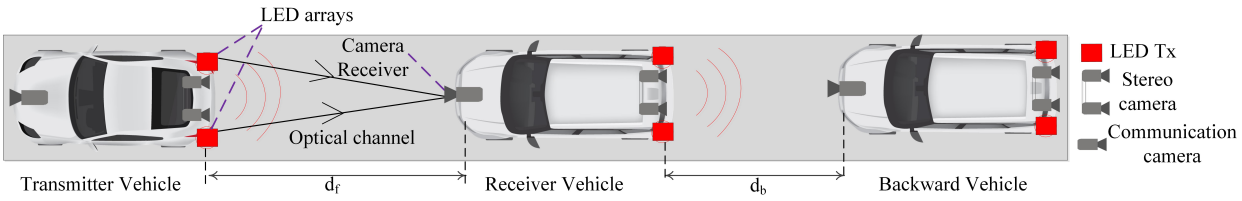

Fig. 2. Proposed system model of vehicular optical camera communication.

B. System Modelling

Fig. 2 outlines the proposed vehicular OCC system model, where vehicles are communicating with each other. In the scenario, the vehicle conveying information is denoted as "Transmitter Vehicle (TV)". Whereas the vehicle which follows the TV and receives the transmitted information is defined as "Receiver Vehicle (RV)". The vehicle located at the back of the RV is termed as "Backward Vehicle". As shown in Fig. 2, the TV sends information using LED lights for communication, which is mainly the vehicle's internal information, e.g., speed, next action, position, and safety and action-related information from other vehicles. The RV detects signals from the LED transmitters using a high frame rate camera (1000 fps in our system). In our system, each vehicle has two camera sets, which measure the vehicle's forward and backward distance and decode the transmitted information from TV. The function of the camera in the front, i.e., high-speed camera, is twofold. Firstly, it measures forward distances between the transmitter and receiver vehicles, and these distances are continuously updated to the processing unit located inside the vehicle. Secondly, the camera acts as the receiver that decodes signal information from the LED transmitters. The camera at the back, i.e., vision camera, measures the backward distance between the vehicles using stereo vision technology [27].

Considering the vehicular network shown in Fig. 2, the measured distance using the high-speed camera is denoted as forward distance, d_{f} and the estimated distance using stereo vision camera is denoted as backward distance, d_{b}. Intensity modulation with direct detection is adopted where the desired waveform is modulated onto the instantaneous power of the LED lights. We consider an adaptive modulation scheme because higher spectral efficiency and lower latency can be achieved by increasing the modulation order. Moreover, higher-order modulation exhibits better BER performance though at the expense of increased bandwidth and power.

C. Optical Channel Model

We assume an uninterrupted LOS link between the transmitter and camera receiver, ensuring the vehicles are free from obstruction in order to communicate with each other continuously. The speed of LED switching frequency is kept high enough so that it is not perceivable by human eye. As a result, LED lights maintain their main purpose of illumination or indication. The camera can receive a signal which lies within their FoV. The radiated signal passes through an optical filter and a lens to ensure maximum light within the FoV of the receiver. Depending on the channel conditions, the OCC channel can be a flat-fading or a diffuse channel. Generally, OCC channel has two types of light propagation components: (i) LOS component resulting from direct light propagation from the transmitter to the receiver and (ii) diffuse components resulting from the reflected lights from other vehicles or reflective surfaces. Usually, the diffuse propagation has much lower energy than the LOS component, and therefore, the diffuse light component is neglected in this paper. Accordingly, considering the visible light LOS channel, the DC gain between the transmitter and receiver is derived by [28] according to

$$H(\theta,t)=\begin{cases}\frac{A_{\text{eff}}(\theta)}{d_{\text{f}}^2(t)}\,\Re(\phi), & 0\le\theta\le\theta_l\\ 0, & \theta>\theta_l\end{cases} \tag{1}$$

where $A_{\text{eff}}(\theta)$ is the effective signal collection area of the image sensor, θ is the angle of incidence (AoI) with respect to the receiver axis, ϕ is the angle of irradiance with respect to the emitter, $\Re(\phi)$ is the transmitter radiant intensity, θ_l denotes the FoV of the image sensor lens, and finally, t is the time-frame index. The distance $d_{\text{f}}(t)$ can be expressed as [21]:

$$d_{\text{f}}(t)=\frac{f}{a}\cdot\frac{\delta}{p(t)}, \tag{2}$$

where δ is the distance between the left and right LED array units, f is the lens focal length, $p(t)$ is the distance in terms of number of pixels between the left and right LED array units on the captured image, and a is the image pixel size. The inter-relation between the distance calculation parameters is illustrated in Fig. 3(a). Whereas, the backward distance d_{b} can be estimated with a stereo vision camera using the same method to the one described in [27].

Regarding the above parameters: δ is sent from the TV to RV through LEDs, and f and a are known values for any system, such as 15 mm and 7.5 μm, in this system. The value of $p(t)$ can be obtained via simple image processing techniques or by calculating the pixel values using data pointer.

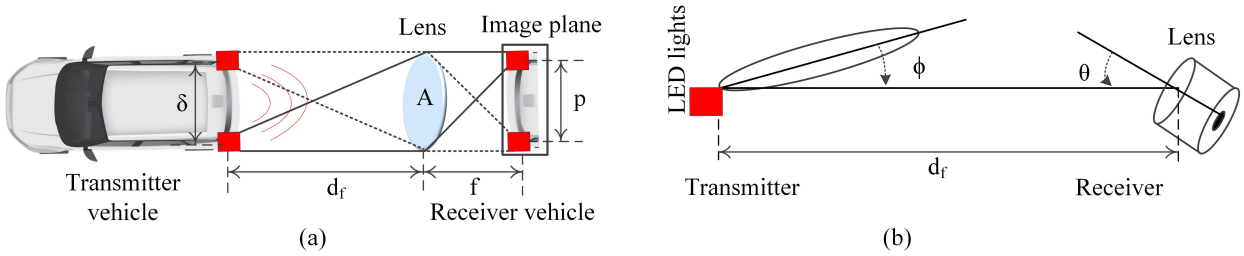

Fig. 3. (a) Inter-vehicular distance measurement [21] and (b) LOS channel model of OCC.

A LED light usually has a Lambertian radiation pattern and wider directivity. Therefore, the light emission from the LED transmitters can be modelled using a generalized Lambertian radiant intensity [28], [29] and following the link geometry, as shown in Fig. 3(b)

$$\Re(\phi) = \frac{(m+1)}{2\pi} \cos^m(\phi), \tag{3}$$

where m is the order of Lambertian emission which is given by the LED semiangle at half luminance $\Phi_{1/2}$:

$$m = \frac{-\ln(2)}{\ln(\cos(\Phi_{1/2}))}. \tag{4}$$

Also, $A_{\text{eff}}(\theta)$ can be expressed as [28]

$$A_{\text{eff}}(\theta) = \begin{cases} A\, T_{\text{s}}(\theta)\, g\, \cos(\theta), & 0 \leq \theta \leq \theta_l \\ 0, & \theta > \theta_l \end{cases} \tag{5}$$

where A is area of the entrance pupil of the camera lens, $T_{\text{s}}(\theta)$ is the signal transmittance of the optical filter, and g is the gain of the lens. An ideal lens with an internal refractive index n has a gain:

$$g = \frac{n^2}{\sin^2(\theta_l)}. \tag{6}$$

Based on the above definitions and considering (3) and (5), finally, (1) can be rewritten as

$$H(\theta, t) = \begin{cases} \frac{(m+1)A}{2\pi d_{\text{f}}^2(t)} \cos^m(\phi)\, T_s(\theta)\, g\, \cos(\theta), & 0 \leq \theta \leq \theta_l \\ 0. & \theta > \theta_l \end{cases} \tag{7}$$

From (7), we observe that if A and g are fixed for an image sensor, the channel power gain $H(\theta, t)$ can be increased by either (a) decreasing the distance, d_{f} and/or (b) increasing the signal collection area, i.e., by decreasing the AoI of the camera lens. Lower AoI of the camera lens means the strength of light beam will be stronger on the image sensor, which in turn, will

increase the channel power gain. Alternatively, higher AoI reduces the $H(\theta, t)$ as the LED light beam will spread out at the wide angle of the camera lens. So, maintaining narrower AoI at the receiver will provide improved performance because of having higher gain.

Finally, the received optical power $P_{\mathrm{r}}(\theta, t)$ can be derived using the optical transmitted power P from LED lights

$$P_{\mathrm{r}}(\theta, t) = P * H(\theta, t). \tag{8}$$

D. Performance Analysis

Motivated by the trade-off between the order of modulation, the achieved BER, and the improved spectral efficiency, we consider adaptive modulation that permits us to adapt modulation order by satisfying minimum BER for the system. It is worth to note that the adjustment of modulation depends on the road scenarios. If the TV wants to transmit any critical information, it may choose a higher modulation based on the size of the transmitted data. On the receiver side, if the RV notices a sudden change in the TV transmitted signal and fails to decode it using the current modulation scheme, the RV switches to another modulation from the chosen set.

From (7), we see that the variables on which the channel gain depends are θ and t. Whereas, t is considered to explain the variation of inter-vehicular distance with time. So, for the sake of studying the impact of the overall system parameters, we replace t with the distance D, i.e., the forward distance. In order to analyze the system performance in terms of BER, spectral efficiency, capacity, and latency, we first formulate the signal-to-noise ratio (SNR) of the optical link. We consider SNR as a measure of communication link quality of the signal transmission. Therefore, according to [30], the received SNR $\gamma(\theta, D)$ of visible light link can be expressed by

$$\gamma(\theta, D) = \frac{P_{\mathrm{r}}^2(\theta, D)}{\sigma^2(\theta, D)} = \frac{P^2 H^2(\theta, D)}{\sigma^2(\theta, D)}. \tag{9}$$

From (7) and (9), we can see that the received SNR depends on θ and D. Therefore, we can control the SNR by constraining D and θ. In (9), $\sigma^2(\theta, D)$ denotes the total noise variance which can be expressed as

$$\sigma^2(\theta, D) = \sigma^2_{\text{shot}}(\theta, D) + \sigma^2_{\text{ther}}, \tag{10}$$

where σ^2_{shot} is the shot-noise variance and σ^2_{ther} is the thermal noise variance [30]. $\sigma^2_{\text{shot}}(\theta, D)$ can be calculated from

$$\sigma^2_{\text{shot}}(\theta, D) = 2qsBP_{\mathrm{r}}(\theta, D) + 2qBI_{\text{bg}}I_2P_n, \tag{11}$$

where q is the electronic charge (1.602×10^{-19} C), B is the equivalent noise bandwidth, s is receiver responsivity, I_{bg} is the background current, P_n is the noise power ($I_{\text{amp}}/R_{\text{b}}$), I_{amp} is the amplifier current, R_{b} is the data rate, and I_2 is the noise bandwidth factor for a rectangular transmitter pulse shape [31].

The thermal noise variance is given by:

$$\sigma^2_{\text{ther}} = \frac{8\pi kT}{G} I_2 B^2 C_f A + \frac{16\pi^2 kT\Gamma}{g_m} I_3 B^3 C_f^2 A^2, \tag{12}$$

where k is Boltzmanns constant, T is absolute temperature, G is the open-loop voltage gain, C_f is the fixed capacitance of the image sensor per unit area, g_m is the FET trans-conductance, Γ is the FET channel noise factor, and I_3 is the noise bandwidth factor [32].

We note that the channel capacity (measured in bit per second (bps)) of a camera based-communication system depends on the received SNR as shown in [14] and is given by

$$C(\theta, D) = W_{\text{fps}}\, W_{\text{s}}(t) \cdot \log_2(1 + \gamma(\theta, D)), \tag{13}$$

where W_{fps} is the camera-frame rate expressed in fps, $W_{\text{s}}(t)$ is the spatial-bandwidth, which can also be denoted by the number of information-carrying pixels per camera image frame. The spatial bandwidth is equivalent to the number of orthogonal or parallel channels in a MIMO system and can be defined by

$$W_{\text{s}}(D) = N_{\text{LEDs}} \times N_{\text{row}}(D), \tag{14}$$

where N_{LEDs} is the number of LEDs at each row of the transmitter and $N_{\text{row}}(D)$ represents the captured number of row pixel lines in each frame. Considering a rolling shutter camera, the actual number of samples $N_{\text{row}}(D)$ acquired from the captured image at distance D can be expressed as

$$N_{\text{row}}(D) = w\, \frac{L_{\text{size}}}{2 \tan\left(\frac{\theta_l}{2}\right) \cdot D}, \tag{15}$$

where w is the image width and L_{size} is LED lights size in cm^2. Taking into account (14) and (15), (13) is re-written as:

$$C(\theta, D) = \frac{W_{\text{fps}}\, N_{\text{LEDs}}\, w\, L_{\text{size}}}{2 \tan\left(\frac{\theta_l}{2}\right) \cdot \frac{1}{d_f}} \cdot \log_2(1 + \gamma(\theta, D)). \tag{16}$$

Considering the communications between the vehicles, the overall E2E latency $\tau(\theta, D)$ can be found as [10]

$$\tau(\theta, D) = \frac{L}{C(\theta, D)}, \tag{17}$$

where L is the packet size in bits. In our system, we consider the E2E latency in terms of transmission latency only and neglect the computational latency because of processing small amount of data. Moreover, the transmission latency depends on the downlink transmission latency, but not on the uplink transmission latency. Because downlink latency is considered for sending the processed task to the RVs and uplink latency is mainly related with requesting a task from the server or other sources by the RVs. In our system, we only send the decision information from TVs to the RVs using back LED lights.

We analyze the capacity for the continuous rate up to now. However, in practice, a certain discrete modulation set is available to examine how the performance varies after limiting the system to a small modulation set. For the considered modulation set, we study binary phase-shift keying (BPSK) and M-ary quadrature amplitude modulation (M-QAM) as an example, but other modulation schemes can also be used. The BER for the optical wireless channel and electrical SNR at the receiver using BPSK, M-QAM can be expressed as [33]:

$$\text{BER}_{\text{BPSK}}(\theta, D) = Q\left(\sqrt{2\gamma(\theta, D)}\right), \tag{18}$$

$$\text{BER}_{\text{M-QAM}}(\theta, D) = \frac{4}{\log_2(M_{\text{n}}(\theta, D))} \cdot Q\left(\sqrt{\frac{3\,\gamma(\theta, D)\,\log_2(M_{\text{n}}(\theta, D))}{M_{\text{n}}(\theta, D) - 1}}\right), \tag{19}$$

where M_{n} is the constellation size (defined as 2^n with n $\geq$ 2) and $Q(x) = \frac{1}{2}\,\text{erfc}\left(\frac{x}{\sqrt{2}}\right)$ stands for the Q function. So, the spectral efficiency of the BPSK and M-QAM modulation schemes can be expressed, respectively, as:

$$\text{SE}_{\text{BPSK}} = 1, \tag{20}$$

$$\text{SE}_{\text{M-QAM}} = \log_2(M_{\text{n}}(\theta, D)), \tag{21}$$

where the spectral efficiency depends on the constellation size, M_{n}, e.g., 1 for BPSK, 2 for 4-QAM. M_{n} is determined by satisfying a target BER at various SNR levels.

Similar to (16) and (17), the channel capacity and E2E latency for the considered discrete modulation set can be written, respectively, as follows:

$$R(\theta, D) = \frac{W_{\text{fps}}\, N_{\text{LEDs}}\, w\, L_{\text{size}}}{2\tan\left(\frac{\theta_l}{2}\right) \cdot \frac{1}{d_f}} \cdot \log_2(M_{\text{n}}(\theta, D)), \tag{22}$$

$$\tau(\theta, D) = \frac{L}{R(\theta, D)}. \tag{23}$$

Typically, AV safety applications are known to be time-critical, as they rely on acquiring updated status from the individual vehicle. For the effective operation of AVs, reliable communication between vehicles is required. This can be achieved, mainly by delivering the information

of the surrounding road environment ahead of reaction time and maintaining regular coordination between AVs, which will, in turn, prevent accidents and ensure road safety. Therefore, our goal is to avoid the critical condition, i.e., avoid collision between vehicles by satisfying uRLLC.

In our system, we vary the inter-vehicular distances and AoIs to investigate the performance of our proposed OCC system. Since it is difficult to change AoI sharply in a realistic scenario as this would introduce additional delays in changing the AoI inside the vehicle, we fix it to a value that satisfies both BER and latency requirements. Hence, we will adapt only the distance D to maximize the capacity.

III. Constrained Problem Formulation

Considering the proposed framework and system requirements, we cast an optimization framework that aims at maximizing the expected capacity through adaptive power allocation while satisfying the reliability and latency requirements. To maintain system integrity, the minimum BER and latency requirements have to be satisfied, whereas the total transmitted power is restricted to a maximum allowable power. As a result, we maximize the capacity of (16) by maximizing

$$\begin{aligned} C\left(D\right) &= \mathbb{E}\left\{\frac{W_{\text{fps}}\ N_{\text{LEDs}}\ w\ L_{\text{size}}}{2\tan\left(\frac{\theta_l}{2}\right)\cdot\ d_f}\cdot\log\left(1+\gamma(D)\right)\right\}, \\ &= \mathbb{E}\left\{l_0.\log\left(1+\gamma(D)\right)\right\}, \end{aligned} \tag{24}$$

where $l_0 = \frac{W_{\text{fps}}\ N_{\text{LEDs}}\ w\ L_{\text{size}}}{2\tan\left(\frac{\theta_l}{2}\right)\cdot d_f}$ and $\mathbb{E}\{\cdot\}$ represents expectation. Since our objective is to maximize capacity through adaptive power allocation, the capacity is not only characterized by distance D but also the transmit power P. Therefore, from hereon, we express the capacity in terms of both P and D.

The average power constraint can be written as

$$\mathbb{E}\{P(D)\} \leq P_{\text{max}}, \tag{25}$$

where P_{max} is the maximum allowable power by our system. Considering the above, (25) can be re-written as

$$\int_0^\infty \frac{P(D)}{P_{\text{max}}} f_d(D) dD \leq 1, \tag{26}$$

where $f_d(D)$ is the probability distribution of D. We use log-normal distribution for the numerical and simulation analysis in our evaluation similar to [34].

Finally, the capacity-maximization problem we study here, can be summarized as:

$$\begin{aligned}
&\max_{\boldsymbol{P(D)}} \quad C(P,D) \\
&= \max_{\boldsymbol{P(D)}} \quad \mathbb{E}\left\{ l_0 \cdot \log\left(1+\frac{P(D)}{P_{\max}}\,\gamma(D)\right)\right\} \\
&= \max_{\boldsymbol{P(D)}} \quad \int_0^{\infty} l_0 \cdot \log\left(1+\frac{P(D)}{P_{\max}}\,\gamma(D)\right)\, f_d(D)dD \qquad (27)\\
&\text{s.t.} \quad \int_0^{\infty} \frac{P(D)}{P_{\max}} f_d(D)dD \le 1, \qquad (28)\\
&\qquad D \ge d_{\text{stop}}, \qquad (29)
\end{aligned}$$

where d_{stop} is the stopping distance, which is equal to the sum of covered distance by the vehicle to travel after the brakes are activated, i.e., braking distance, and the covered distance to travel due to driver reaction time, i.e., reaction distance, to react after observing a situation [35]. Constraint (28) indicates that the expected power is maintained at least $P_{\max}$. Constraint (29) ensures that the forward distance does not fall beyond d_{stop}. Although the maximization problem does not include the backward distance d_{b}, it is constrained by $d_{\text{b}} \ge d_{\text{stop}}$, in order to avoid collision with the vehicle behind.

Lemma 1: The optimization problem described by (27) is a concave optimization problem with respect to P.

Proof: Please see Appendix A.

IV. Proposed Solution

A. Solution of the Problem with Lagrangian Formulation

In Appendix A, we have proved that the optimization objective function is concave. Hence, the adaptive solution to this problem may be found with the Lagrangian relaxation. The Lagrangian relaxation for (27) under the constraint of (28) and (29) can be expressed as:

$$\begin{aligned}
\mathcal{L}(P(D),\lambda,\mu) = l_0 \int_0^{\infty} \log\left(1+\frac{P(D)}{P_{\max}}\gamma(D)\right) f_d(D)dD - \lambda\left[\int_0^{\infty}\frac{P(D)}{P_{\max}} f_d(D)dD - 1\right] \\
- \mu(D-d_{\text{stop}}), \qquad (30)
\end{aligned}$$

where λ and μ are Lagrange multipliers associated with (28) and (29). We get the expression of power allocation by letting the derivative of (30) with respect $P(D)$ be zero, as follows

$$\frac{\partial\mathcal{L}(P(D),\lambda,\mu)}{\partial(P(D))} = l_0 \int_0^{\infty} \frac{\frac{\gamma(D)}{P_{\max}}}{1+\frac{P(D)}{P_{\max}}\,\gamma(D)}\, f_d(D)dD - \lambda\int_0^{\infty}\frac{1}{P_{\max}} f_d(D)dD = 0, \qquad (31)$$

$$\Rightarrow \frac{P(D)}{P_{\max}} = \frac{1}{\gamma_0} - \frac{1}{\gamma(D)}, \tag{32}$$

where $\gamma_0 = \frac{\lambda}{l_0}$. From (32), the power allocation that maximizes (27) can be written for some threshold value γ_0 as

$$\frac{P(D)}{P_{\max}} = \begin{cases} \frac{1}{\gamma_0} - \frac{1}{\gamma(D)}, & \gamma(D) \geq \gamma_0 \\ 0, & \gamma(D) < \gamma_0 \end{cases} \tag{33}$$

Since γ varies with distance, the distribution of transmit power (33) follows a water-filling formula, which depends on γ_0. In particular, when the channel is strong, i.e., $\gamma(D)$ is large enough to satisfy the link quality, more power is allocated to that link for data transmission. Conversely, if the channel quality drops below γ_0, no power is allocated to that time of data transmission, which means the channel will not be used.

Substituting (33) into (26), γ_0 can be determined by solving

$$\int_0^{\infty} \left(\frac{1}{\gamma_0} - \frac{1}{\gamma(D)} \right) f_d(D) dD = 1. \tag{34}$$

Using the distributions of $f_d(D)$, a closed-form representation of γ_0 can be found. Once γ_0 is determined, by substituting (33) into (27), we find the capacity as

$$\max_{\boldsymbol{P(D)}} \int_0^{\infty} l_0 \cdot \log \left(\frac{\gamma(D)}{\gamma_0} \right) f_d(D) dD. \tag{35}$$

Using (34) and (35), the adaptive solution of expected capacity can be determined in vehicular OCC.

B. Problem Transformation

In order to analyze the performance of the proposed solution using the considered discrete modulation set, we re-express the main problem in (27) into a discrete problem. In general, Shannon's capacity analysis does not give an indication on how to design adaptive or non-adaptive techniques for real systems. Once the rate and associated power are allocated, we may find the constellation size for the chosen modulation set while satisfying the BER and

latency requirements. Therefore, the discrete capacity optimization problem can be rewritten by considering uRLLC and modulation set constraints as follows:

$$\max_{\boldsymbol{P(D)},\boldsymbol{M}_{\text{n}}} \quad \mathbb{E}\left\{R(P,D)\right\}$$

$$= \max_{\boldsymbol{P(D)},\boldsymbol{M}_{\text{n}}} \quad \mathbb{E}\left\{\frac{W_{\text{fps}}\ N_{\text{LEDs}}\ w\ L_{\text{size}}}{2\tan\left(\frac{\theta_l}{2}\right)\cdot\ d_f}\cdot\log_2(M_{\text{n}}(D))\right\} \tag{36}$$

$$\text{s.t.} \quad \mathbb{E}\{P(D)\} \leq P_{\text{max}}, \tag{37}$$

$$D \geq d_{\text{stop}}, \tag{38}$$

$$I(\text{BER}(D) \leq 10^{-4}) = 1, \tag{39}$$

$$I(\tau(D) \leq 10\text{ms}) = 1, \tag{40}$$

$$M_{\text{n}} \in \{\text{BPSK}, \{4,8,16,32,64\} - \text{QAM}\}, \tag{41}$$

where $I(\cdot)$ is an indicator function. Constraints (39) and (40) indicate that the reliability and latency is satisfied for ensuring uRLLC. The modulation scheme is chosen from a small set of available modulations, which is restricted by the constraint (41). Ideally, the transmit power associated with each region (defined by γ range) should be optimized to maximize capacity for each constellation M_{n}. However, since we do not have a closed-form expression for the discrete capacity, we perform an exhaustive search to find the solution to the problem.

Since the power adaptation is continuous where the constellation size is discrete, we need to adjust the constellation size while satisfying the uRLLC requirements. For each value of P, we must decide the suitable γ and constellation size to transmit. The choice of γ and constellation size by the transmitter is analyzed as follows. We determine the constellation size associated with each P by discretizing γ into different levels. Specifically, we divide the range of γ into various regions, which satisfies the BER target and latency requirements. The data rate for the certain γ region is thus characterized as $\log_2(M_{\text{n}})$, and hence, it defines the optimal constellation size for each γ. In this manner, we find an adaptive solution of maximized expected capacity using adaptive power allocation and a certain modulation set while satisfying the uRLLC requirements in the vehicular OCC.

V. Simulation Results and Performance Analysis

In this section, simulations are conducted to investigate the performance of the proposed system model and capacity optimization method in vehicular OCC. We evaluate the effect of the

TABLE II

SIMULATION PARAMETERS

Parameter, Notation	Value	Parameter, Notation	Value
Angle of irradiance w.r.t. the emitter, ϕ	70^o	Boltzmanns constant, k	1.3807×10^{-23}
Semi-angle at half luminance of the LED, $\Phi_{1/2}$	60^o	Absolute temperature, T	298 K
Inter-vehicular distance, d_{f}	$(0 - 150)$ m	Open loop voltage gain, G	10
AoI w.r.t. the receiver axis, θ	0^o to 90^o	Fixed capacitance, C_f	112×10^{-8}
FoV of the camera lens, θ_l	90^o	FET channel noise factor, Γ	1.5
Image sensor physical area, A	10 cm^2	FET trans-conductance, g_m	30 ms
Transmission efficiency of the optical filter, T_s	1	Noise bandwidth factor, I_3	0.0868
Refractive index of concentrator/lens, n	1.5	Constellation size, M_{n}	4, 8, 16, 32, and 64
Background current, I_{bg}	5100 μA	Camera-frame rate, W_{fps}	1000 fps
Optical transmitting power, P	1.2 Watts	Amplifier current, I_{amp}	5 pA
Focal length of the camera lens, f	15 mm	Electron charge, q	1.6×10^{-19} C
Equivalent noise/electronic bandwidth, B	2 MHz	Image pixel size, a	7.5 μm
Noise bandwidth factor for a rectangular pulse, I_2	0.562	Size of the LED, L_{size}	15.5 $\times$ 5.5 cm^2
Number of LEDs in the transmitter, N_{LEDs}	300 (30 $\times$ 10)	Resolution of image, w	512 $\times$ 512 pixels
Data rate of system, R_{b}	500 bps	Packet size, L	5 kbits

proposed system on different performance metrics to get a better understanding of the interplay among the various parameters of our system. We consider adaptive modulation scheme with BPSK and M-QAM with five different constellations, $M_{\text{n}} = \{4, 8, 16, 32, 64\}$. Target BER is set to 10^{-4} and 10^{-5} for performance comparison to be compliant with uRLLC requirements while setting E2E latency to 10 ms. In order to justify the robustness of the proposed method, we simulate the optimization model using the water-filling algorithm. Finally, we analyze the performance of the proposed power and modulation allocation scheme for capacity and latency. We consider a transmitter of 300 (30 $\times$ 10) LEDs and a 1000 fps high-speed camera for the receiver where the resolution of the received image is assumed to be 512$\times$ 512. The rest of the simulation-related parameters are summarized in Table II.

1) Performance of BER Modelling: In this sub-section and the following sub-section, we analyze the performance of the proposed system model in terms of BER, spectral efficiency, and latency at different inter-vehicular distances and AoIs. In this manner, we aim at justifying that our proposed system offers better performance at various target BER using the chosen modulations. We start by comparing the BER performance versus SNR (dB) for the chosen

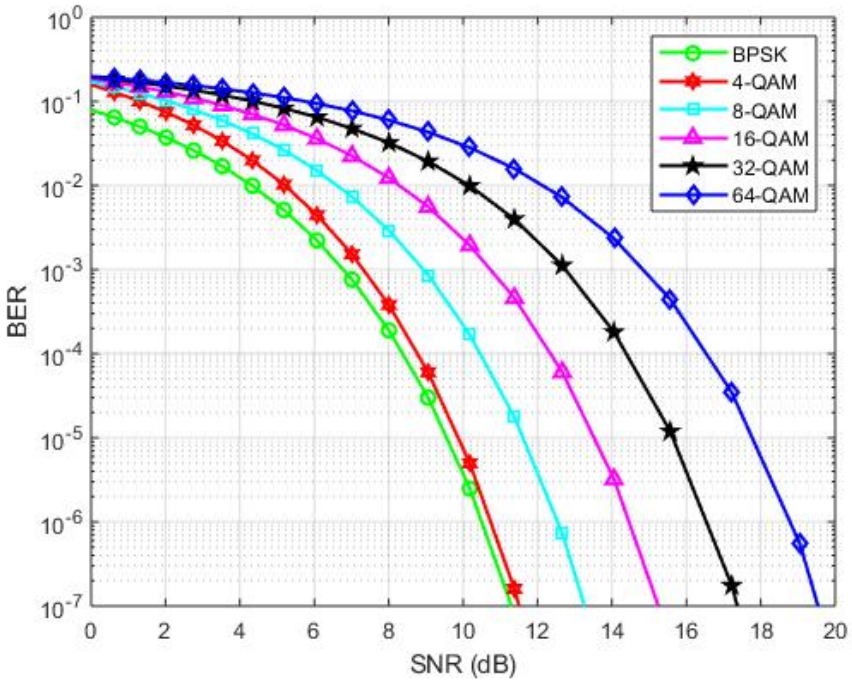

Fig. 4. BER versus SNR (dB) for various modulation schemes considering AoI = 60^0 and fixed transmit power at 1.2 W, when d_{f} is varying.

modulation scheme with a fixed transmit power of 1.2 Watt. The results are illustrated in Fig. 4 and Fig. 5, which show the comparison at different inter-vehicular distances and AoIs, respectively. The results show that we get better BER performance at higher-order modulation, but at the cost of high SNR level. In our evaluation, we do not vary the distance and AoI at the same time. During varying distance, we change it from 0 m to 150 m by keeping the AoI at 60^o, whereas we vary AoIs between 0^o to 90^o by keeping the distance to 50 m. We note that the same BER performance can be achieved at various distances and AoIs by using different modulation schemes.

In Fig. 6 and Fig. 7, we evaluated the achieved BER performance for the different modulation schemes at varying distances and AoIs, respectively. Fig. 6 shows that BPSK satisfies target BER (10^{-4}) up to 82 m, and for 64-QAM, it is satisfied at 52 m. Similarly, in Fig. 7, target BER (10^{-4}) is satisfied at 80^o and 62^o for BPSK and 64-QAM, respectively. At the narrower AoI, the strength of light beam on the image sensor is strong, which increases channel gain. Alternatively, at the shorter distance, the SNR gets higher. Therefore, at shorter distance and

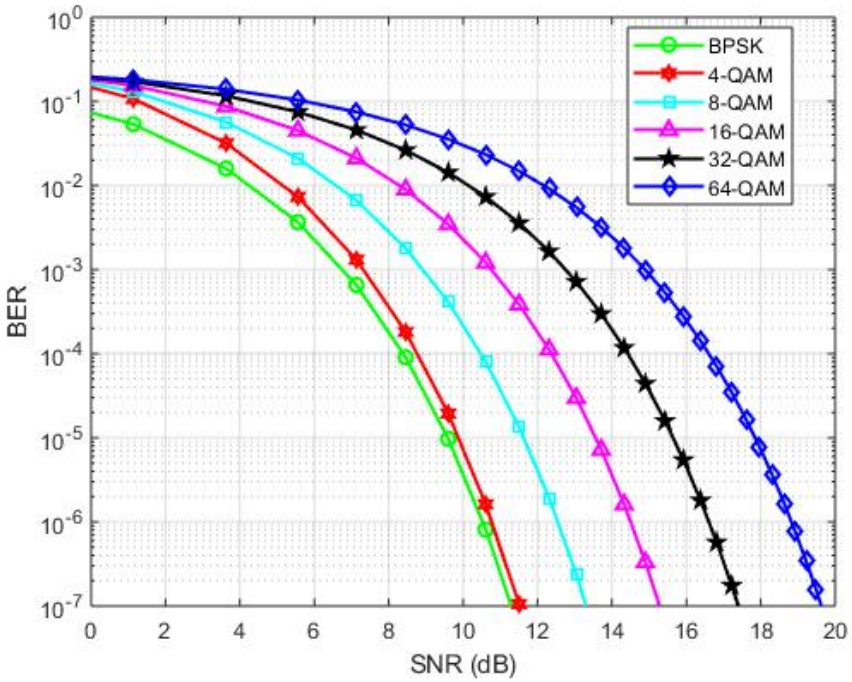

Fig. 5. BER versus SNR (dB) for various modulation schemes considering d_f = 50 m and fixed transmit power at 1.2 W, when AoI is varying.

narrower AoI, the modulation order will be higher due to higher SNR at the receiver.

2) Spectral Efficiency and Latency Performance: The achieved spectral efficiency and observed latency improvements by the proposed system at various distance values are presented in Fig. 8. In this evaluation, we consider, 10^{-4} and 10^{-5}, as the target BER for performance comparison. We determine the distance that satisfies the target BER, and then, adopt the highest modulation scheme from all the available schemes using Fig. 6 and (21). Then, we calculate the spectral efficiency at that corresponding modulation scheme and distance. We achieve spectral efficiency of 6 bps/Hz (Fig. 8) for distance until 48 m (for BER = 10^{-5}) and 52 m (for BER = 10^{-4}) using 64-QAM. Likewise, we notice a spectral efficiency of 2 bps/Hz from 74 m to 81 m and 69 m to 76 m at the target BER of 10^{-4} and 10^{-5}, respectively. Please note that the above evaluation is ideal since it assumes that the modulation level is perfectly adapted and the probability of error is known beforehand and is accurate.

For latency evaluation, we first calculate the capacity using (22), considering that the camera captures images with resolution of 512×512 pixels. Then, we estimate the achievable transmission latency for the transmission of packets with size 5 kbits using (23). Here, we consider

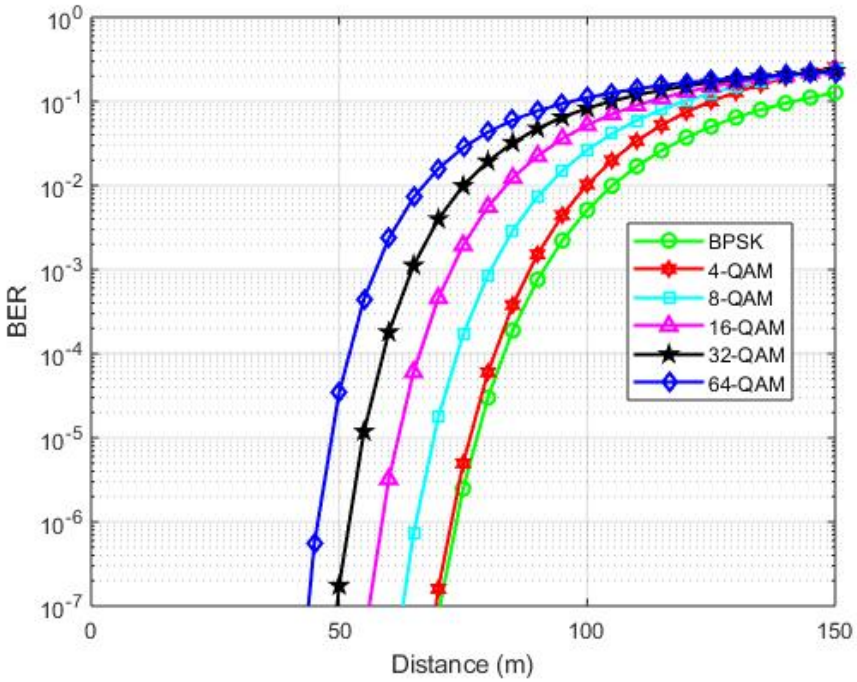

Fig. 6. BER versus Distance (m) for various modulation schemes considering AoI = 60^0 and fixed transmit power at 1.2 W.

transmission latency as E2E latency because we process small amount of data in our system. The results are presented in Fig. 8 at distance between 0 m to 90 m while satisfying two different target BERs, i.e., 10^{-4} and 10^{-5}. This evaluation shows that our system can achieve the latency of uRLLC, which is around 1ms at 52 m and 48 m at target BER of 10^{-4} and 10^{-5}, respectively. From the analysis of Fig. 7, we see that at 60^0 of AoI, our system satisfies the target BER of 10^{-4} using 64-QAM modulation scheme. From Fig. 8, it can be seen that we can achieve 1ms latency and spectral efficiency of 6 bps/Hz using 64-QAM. So, we note that both latency and BER requirements are satisfied at 60^0. As a result, we consider AoI as 60^0 for the formulation of our optimization problem in order to avoid the complexity of changing AoI in practice and its induced latency.

From Fig. 8, we can conclude that the use of adaptive modulation offers higher spectral efficiency and lower latency. Whereas, a single modulation scheme offers fixed-rate and latency having limitations in distance coverage and target BER. For example, 64-QAM can satisfy a target BER of 10^{-4} and a latency of 1.2ms up to 52 m. Thus, beyond this distance, we need another modulation scheme for satisfying the target BER, i.e., 32-QAM, 16-QAM, and so on.

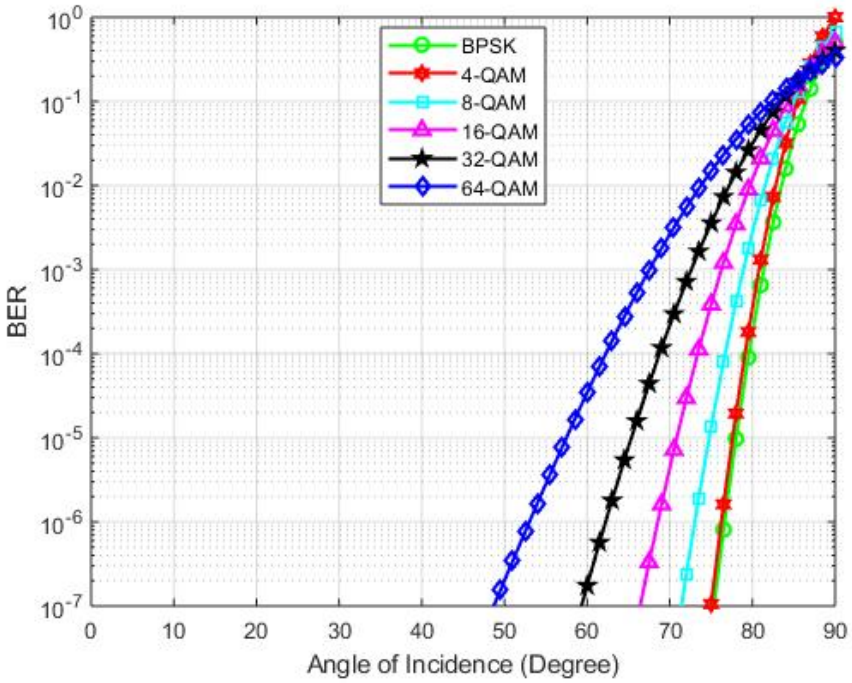

Fig. 7. BER versus AoI (Degree) for M-QAM scheme considering d_t = 50 m and fixed transmit power at 1.2 W.

Similarly, BPSK satisfies the target BER up to 83 m but offers a lower rate, i.e., 1 bps/Hz and higher latency of 7.5ms. Accordingly, it can be said that adaptive modulation provides better performance while satisfying the trade-off between reliability and latency requirements at different modulation schemes and distances.

3) Performance of Optimization Solution: To analyze the impact of using the proposed scheme on the average capacity, we compare the average capacity with average latency under various rate and power allocation, namely continuous rate and power, discrete rate and continuous power, and constant power methods as shown in Fig. 9. It is seen that with the increase of latency, the capacity of each scheme degrades due to the limited availability of data at a higher latency. We perform 10^5 iterations to evaluate the average capacity in our simulation, which is based on Monte-Carlo simulation. Then, we compute the transmission latency for a packet size of 5 kbits. The inter-vehicular distance is formulated as the log-normal distribution for our evaluation considering the mean as $\log(50)$ and the standard deviation as 1.

For continuous rate, we allocate the power using the water-filling algorithm of (33) to find the adaptive solution while satisfying the target BER, i.e., 10^{-4} using (35). For discrete rate,

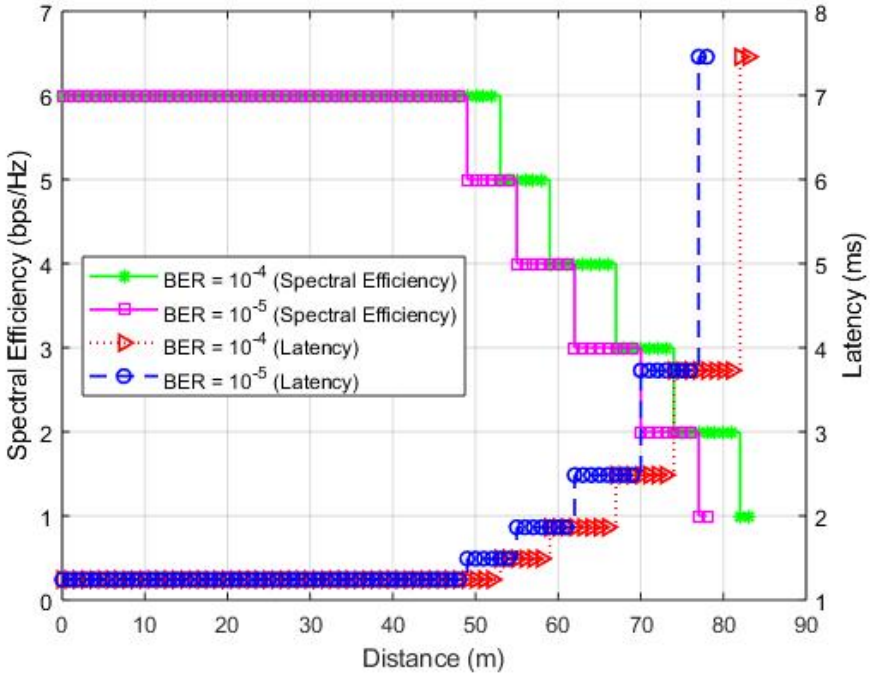

Fig. 8. Spectral efficiency and latency versus distance at target BER of 10^{-4} and 10^{-5}.

TABLE III

VALUES OF RECEIVED SNR, WHEN TARGET BER IS 10^{-4} AND 10^{-5}

Mn	BPSK	4	8	16	32	64
γ(dB) when BER = 10^{-4}	8.4 - 8.75	8.75 - 10.5	10.5 - 12.3	12.3- 14.45	14.45 - 16.55	16.5 - ∞
γ(dB) when BER = 10^{-5}	9.55 - 9.85	9.85 - 11.6	11.6 - 13.5	13.5 - 15.65	15.65 - 17.8	17.8 - ∞

we choose a certain modulation set in which the reliability requirements are satisfied using (36). For non-optimized capacity, we evaluate the capacity considering continuous rate and constant transmit power. From Fig. 9, we see that the average capacity of the optimized method using adaptive power allocation outperforms the non-optimized capacity scheme. For discrete and continuous capacity, the performance of capacity over latency exhibits almost a similar characteristic. For discrete policy, there is no closed-form solution for the capacity and latency, and hence, the solution is found using an exhaustive search technique. The capacity is obtained by determining the value of M_{n} while satisfying the target BER of 10^{-4} for a given power level. Using the transmit power, we can determine received SNR, and hence, the corresponding M. For example, as shown in Fig. 4, for 64-QAM, the target BER is satisfied at 16.5 dB which

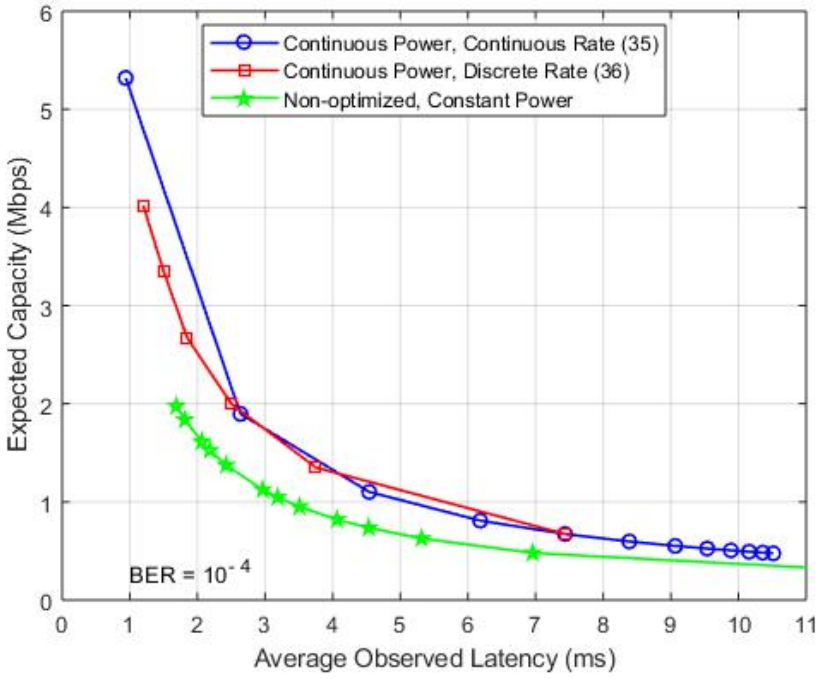

Fig. 9. Expected capacity versus observed latency at various rate and power allocation while satisfying the target BER = 10^{-4}.

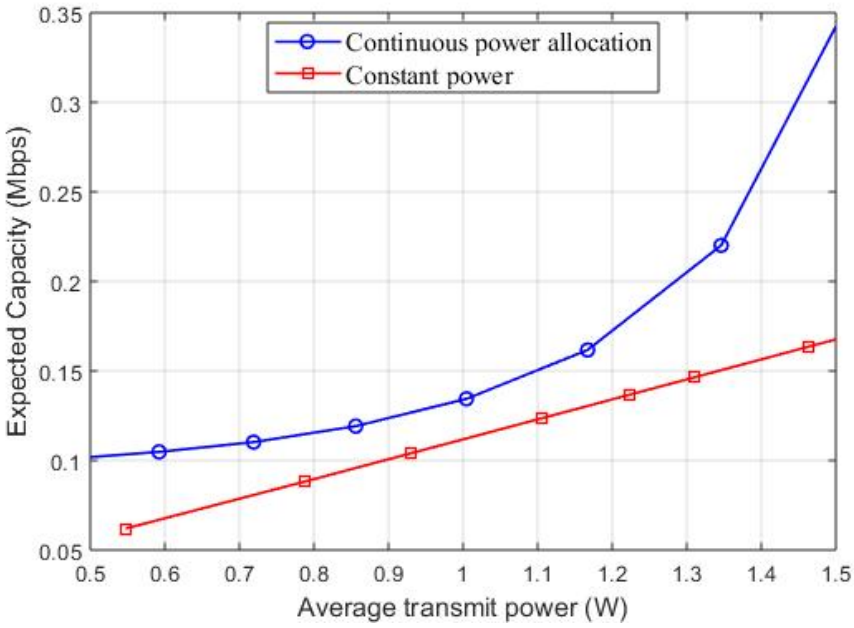

Fig. 10. Average capacity versus transmit power.

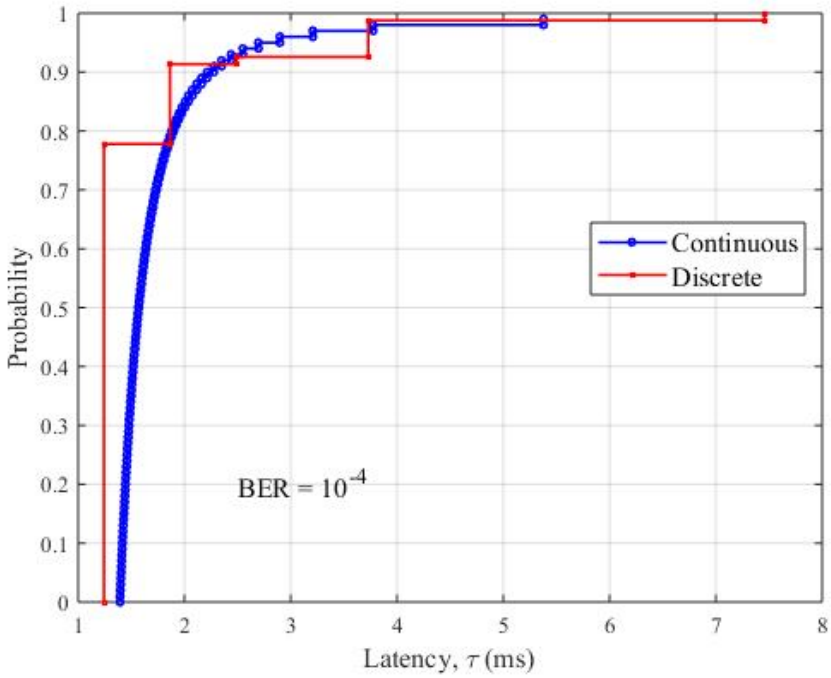

Fig. 11. Probability of latency for continuous and discrete rate while satisfying target BER of 10^{-4}.

corresponds to 52 m distance (Fig. 6). Then, the capacity and latency are evaluated based on the modulation scheme at the satisfied SNR and distance level. The values of received SNR at different constellation sizes are shown in Table III, where SNR levels are determined using Fig. 4 when the target BERs are 10^{-4} and 10^{-5}.

Whereas, the expected capacity with respect to average transmit power is evaluated for both continuous and constant power in Fig. 10. We allocate power using water-filling algorithm for continuous. We notice an increase in the capacity with the increase of transmit power. It is seen that the capacity remains almost similar until 1.2 Watt, then the average capacity increases quickly for continuous rate allocation. Because when more power is allocated to the communication link, the link quality gets better, which increases the expected capacity consequently. But for constant power, the capacity remains almost identical for all the power values as there is no power allocation mechanism depending on the link quality.

In order to show the impact of both continuous and discrete rate on the overall E2E latency, the cumulative distribution function (CDF) of these metrics is shown in Fig. 11. We evaluate the CDF of E2E latency for the proposed vehicular network while satisfying the target BER, i.e., 10^{-4}.

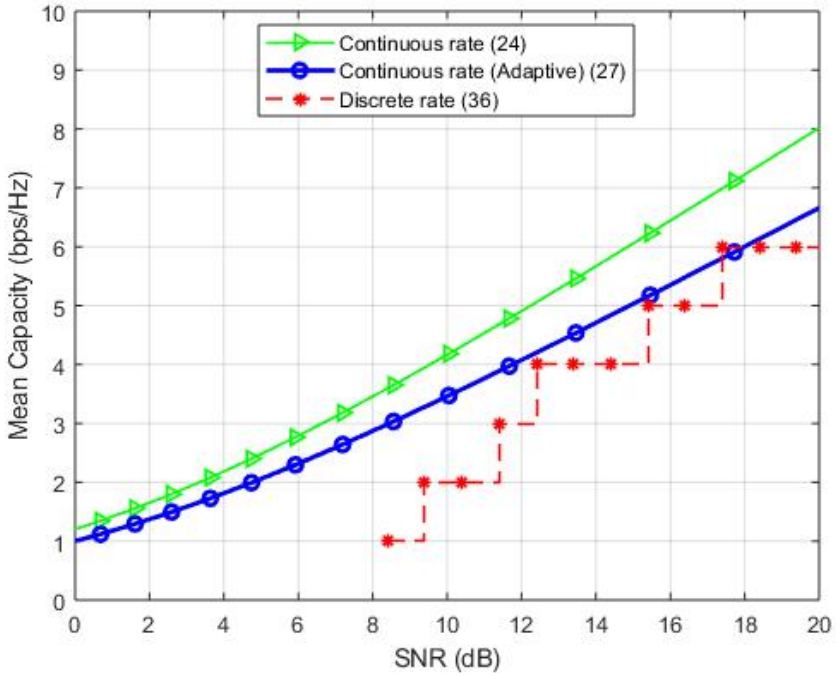

Fig. 12. Capacity versus SNR (dB) for different rate satisfying uRLLC under various considered approaches.

First, we observe that the proposed scheme can guarantee a quite similar latency characteristic until 5.5ms despite the two different rates. Both representations can guarantee 5.5ms E2E latency with a high probability close to 99%. It also yields that the probability latency is strictly less than the required maximum latency, i.e., 10ms. This proves that the proposed scheme can satisfy the latency requirement of the proposed V2V communication while maintaining the reliability requirement.

Finally, we compare the maximized expected capacity performance of discrete (for the chosen modulation set) and continuous rate as a function of different SNR ranges while satisfying the BER and latency requirements, as shown in Fig. 12. With the rise of received SNR, the expected capacity increases due to higher channel gain at the receiver. It is seen if the received SNR is more than 12 dB, the achieved capacity values are very close to each other when the problem is solved by continuous and discrete rate optimization method. We note that the discrete scheme shows a similar performance when the chosen modulation order has higher constellation and SNR level. This justifies that the computed capacity values are not affected by considering a discrete set instead of continuous though it satisfies the uRLLC requirements. This demonstrates

the effectiveness and the convergence of the proposed optimization scheme in vehicular OCC.

VI. Conclusion

In this paper, we present a capacity maximization method in vehicular OCC through adaptive power allocation subject to latency and reliability constraints. First, we analyze the proposed channel model and several performance metrics where the latency is modelled as transmission latency only and reliability is modelled by satisfying the target BER, i.e., 10^{-4} and 10^{-5}. We carried numerous simulations to get an understanding of how to adjust the employed modulation scheme as well as AoIs so that it meets the BER and latency requirements. Then, we fixed the AoI at 60^0 in order to reduce the complexity of changing physical AoI and avoid induced latency for it. Then, the capacity optimization problem is formulated considering the uRLLC constraints, and the solution is proposed with the help of a Lagrangian formulation and water-filling algorithm. Finally, we justify the performance of our proposed optimization method for a small set of discrete modulation scheme. We compare the performance of joint modulation and power allocation strategies through simulation results to validate the convergence of the proposed methodology. Simulation results show that the proposed method provides similar performance for both discrete and continuous policy in terms of average capacity, observed latency, and received SNR. Therefore, our proposed optimization scheme shows the robustness in terms of system performance by satisfying the uRLLC requirements even after considering a small set of modulation scheme.

Appendix A
Proof of Lemma 1

In this appendix, we prove Lemma 1. For this purpose, we express our objective function of (24) as[2]

$$\begin{aligned} C\left(P,D\right) &= l_0 \cdot \log\left(1+\gamma(P)\right) \\ &= l_0 \cdot \log\left(1+\frac{P^2H^2}{2qBsHP+2qBI_{\text{bg}}I_2P_n+\sigma^2_{\text{ther}}}\right). \end{aligned} \tag{42}$$

For the sake of simplicity of representation, we consider $k = H^2$, $z = 2qBsH$, $w = 2qBI_{\text{bg}}I_2P_n + \sigma^2_{\text{ther}}$. Substituting these into (42), we get

$$C(P,D) = l_0 \cdot \log\left(1+\frac{kP^2}{zP+w}\right). \tag{43}$$

[2]For simplicity of representation, we use P instead of $P(D)$ in this proof.

To ensure that $C(P,D)$ is concave with respect to P, we need to satisfy that $\frac{\partial^2 C(P,D)}{\partial P^2} \leq 0$. Hence, we express $\frac{\partial^2 C(P,D)}{\partial P^2}$ as

$$\frac{\partial^2 C(P,D)}{\partial P^2} = l_0 \cdot k \cdot \frac{-kz^2P^4 - 4kzwP^3 - 2kw^2P^2 + 2zw^2P + 2w^3}{(kP^2 + zP + w)^2(zP + w)^2}. \tag{44}$$

Now, we express (43) in terms of $U(P)$ as

$$C(P,D) = l_0 \cdot \log\left(U(P)\right), \tag{45}$$

where $U(P) = 1 + \frac{kP^2}{zP+w}$. Similar to (44), to satisfy the concavity condition, $\frac{\partial^2 C(P,D)}{\partial P^2}$ can be expressed as

$$\begin{aligned}\frac{\partial^2 C(P,D)}{\partial P^2} &= l_0 \cdot \frac{\frac{\partial^2 U(P)}{\partial P^2}\, U(P) - \left(\frac{\partial U(P)}{\partial P}\right)^2}{U^2(P)}, \\ &= l_0 \cdot \frac{g(P)}{U^2(P)},\end{aligned} \tag{46}$$

where $g(P) = \frac{\partial^2 U(P)}{\partial P^2}\, U(P) - \left(\frac{\partial U(P)}{\partial P}\right)^2$.

Therefore, if we can prove $g(P) \leq 0$, then $\frac{\partial^2 C(P,D)}{\partial P^2} \leq 0$, which guarantees the concavity, since $U^2(P)$ is positive. To justify the behavior of $g(P)$, we determine the sign of $g(P)$ by taking the first derivative of $g(P)$ with respect to P as

$$\frac{\partial g(P)}{\partial P} = \frac{\partial^3 U(P)}{\partial P^3}\, U(P) - \frac{\partial U(P)}{\partial P} \cdot \frac{\partial^2 U(P)}{\partial P^2}. \tag{47}$$

We can find the sign of (47) by taking first, second, and third partial derivative of $U(P)$ with respect to P, respectively, as

$$\frac{\partial U(P)}{\partial P} = \frac{k\left(zP^2 + 2wP\right)}{\left(zP + w\right)^2}, \tag{48}$$

$$\frac{\partial U^2(P)}{\partial P^2} = \frac{2kw^2}{\left(zP + w\right)^3}, \tag{49}$$

$$\frac{\partial U^3(P)}{\partial P^3} = \frac{-6kzw^2}{\left(zP + w\right)^4}. \tag{50}$$

For any value of P, we see that $\frac{\partial U(P)}{\partial P} > 0$, $\frac{\partial^2 U(P)}{\partial P^2} > 0$, and $\frac{\partial^3 U(P)}{\partial P^3} < 0$, which implies $\frac{\partial g(P)}{\partial P} < 0$ and proves that $U(P)$ is always a decreasing function with respect to P.

Considering (44) and (46), we get

$$g(P) = k\left(-kz^2P^4 - 4kzwP^3 - 2kw^2P^2 + 2zw^2P + 2w^3\right). \tag{51}$$

We see that all terms in (51) are negative, but the last two terms and its value is determined as follows

$$g(P)|_{P=0} = 2kw^3 \approx 0. \tag{52}$$

As a result, $g(P)$ can be assumed to be negative for $P \geq 0$. Therefore, the second derivative of $C(P, D)$ is always negative for $P \geq 0$ and we conclude that $C(P, D)$ is a concave function.

REFERENCES

[1] Mckinsey and Company, "The Road to 2020 and Beyond-Whats driving the global automotive industry," 2013.

[2] A. E. Fernandez and M. Fallgren, "5GCAR scenarios, use cases, requirements and KPIs," *Fifth Generation Communication Automotive Research and innovation*, Tech. Rep. D2.1, Aug. 2017.

[3] S. h. Sun, J. l. Hu, Y. Peng, X. m. Pan, L. Zhao, and J. y. Fang, "Support for vehicle-to-everything services based on LTE," *IEEE Wireless Commun.*, vol. 23, no. 3, pp. 4-8, June 2016.

[4] C. Liu and M. Bennis, "Ultra-reliable and low-latency vehicular transmission: An extreme value theory approach," *IEEE Commun. Lett.*, vol. 22, no. 6, pp. 1292-1295, June 2018.

[5] M. I. Ashraf, Chen-Feng Liu, M. Bennis, and W. Saad, "Towards low-latency and ultra-reliable vehicle-to-vehicle communication, in *Proc. EuCNC*, Oulu, Finland, June 2017, pp. 1-5.

[6] W. Sun, E. G. Strom, F. Brannstrom, Y. Sui, and K. C. Sou, "D2D-based V2V communications with latency and reliability constraints," in *Proc. IEEE GC Wkshps*, Dec. 2014, pp. 1414-1419.

[7] K. Lee, J. Kim, Y. Park, H. Wang, and D. Hong, "Latency of cellular-based V2X: Perspectives on TTI-proportional latency and TTI-independent latency," *IEEE Access*, vol. 5, pp. 15800-15809, Jul. 2017.

[8] J. Park and P. Popovski, "Coverage and rate of downlink sequence transmissions with reliability guarantees," *IEEE Wireless Commun. Lett.*, vol. 6, no. 6, pp. 722-725, Dec. 2017.

[9] P. Popovski et al., "Wireless access for ultra-reliable low-latency communication: Principles and building blocks," *IEEE Netw.*, vol. 32, no. 2, pp. 16-23, Apr. 2018.

[10] Md M. K. Tareq, O. Semiari, M. A. Salehi, and W. Saad, "Ultra Reliable, Low Latency Vehicle-to-Infrastructure Wireless Communications with Edge Computing," *ArXiv*, Aug. 2017.

[11] W. Shi and S. Dustdar, "The promise of edge computing," *Computer*, vol. 49, no. 5, pp. 78-81, May 2016.

[12] L. Zeng et al., "High data rate multiple input multiple output (MIMO) optical wireless communications using white LED lighting," *IEEE J. Sel. Areas Commun.*, vol. 27, no. 9, pp. 1654-1662, Dec. 2009.

[13] R. Mesleh, H. Elgala, and T. D. C. Little, "A novel method to mitigate LED nonlinearity distortions in optical wireless OFDM systems," in *Proc. OFC/NFOFC*, Mar. 2013, pp. 1-3.

[14] A. Ashok, S. Jain, M. Gruteser, N. Mandayam, W. Yuan, and K. Dana, "Capacity of screen-camera communications under perspective distortions," *Pervasive Mob. Comput.*, no. 16, pp. 239-250, Jan. 2015.

[15] T. Yamazato et al., "Image-sensor-based visible light communication for automotive applications," *IEEE Commun. Mag.*, vol. 52, no. 7, pp. 88-97, Jul. 2014.

[16] J. Barbaresso, G. Cordahi, D. E. Garcia, C. Hill, A. Jendzejec, and K. Wright, "USDOTs Intelligent transportation systems (ITS) ITS strategic plan 2015-2019," *US Department of Transportation, Intelligent Transportation Systems*, Joint Program Office, Washington, DC, USA, 2015.

[17] S. Al-Sultan, M. M. Al-Doori, A. H. Al-Bayatti, and H. Zedan,, "A comprehensive survey on vehicular Ad Hoc network," *J. Netw. and Comp. Applications*, vol. 37, no. 1, pp. 380-392, Jan. 2014.

[18] S. Bitam, A. Mellouk, and S. Zeadally, "VANET-cloud: A generic cloud computing model for vehicular ad hoc networks," *IEEE Wireless Commun.*, vol. 22, no. 1, pp. 96-102, Feb. 2015.

[19] F. A. Teixeira, et al. "Vehicular networks using the IEEE 802.11p standard: An experimental analysis," *Veh. Commun.* vol. 2014, no.1, pp. 91-96, Apr. 2014.

[20] S. Okada, et al. "On-vehicle receiver for distant visible light road-to-vehicle communication," in *Proc. IEEE Intell. Veh. Symp.*, pp. 1033-1038, Jun. 2009.

[21] I. Takai, et al. "Optical vehicle-to-vehicle communication system using LED transmitter and camera receiver," *IEEE Photon. J.*, vol. 6, no. 5, pp. 1-14, Oct. 2014.

[22] A. Islam, L. Musavian, and N. Thomos, "Performance Analysis of Vehicular Optical Camera Communications: Roadmap to uRLLC," in *Proc. 2019 GlobeCom*, Hawaii, United States, Dec. 2019. (Accepted)

[23] T. Yamazato et al., "Vehicle motion and pixel illumination modeling for image sensor based visible light communication," *IEEE J. Sel. Areas Commun.*, vol. 33, no. 9, pp. 1793-1805, Sep. 2015.

[24] T. Nguyen, A. Islam, and Y. M. Jang, "Region-of-interest signaling vehicular system using optical camera communications," *IEEE Photon. J.*, vol. 9, no. 1, pp. 1-20, Feb. 2017.

[25] W. Travis, A.T. Simmons, and D.M. Bevly, "Corridor navigation with a LiDAR/INS Kalman filter solution," in *Proc. IEEE Intell. Veh. Symp.*, Las Vegas, NV, USA, pp. 343-348, 2005.

[26] I. Takai, et al. "LED and CMOS image sensor based optical wireless communication system for automotive applications," *IEEE Photon. J.*, vol. 5, no. 5, pp. 6801418-6801418, Oct. 2013.

[27] A. Islam, M. T. Hossan, and Y. M. Jang, "Convolutional Neural Network Scheme-Based Optical Camera Communication System for Intelligent Internet of Vehicles," *Int. J. of Distributed Sensor Netw.*, vol. 14, no. 4, pp. 1-19, Apr. 2018.

[28] J. Kahn and J. Barry, "Wireless infrared communications," *Proc. IEEE*, vol. 85, no. 2, pp. 265-298, Feb. 1997.

[29] Z. Ghassemlooy, D. Wu, M. A. Khalighi, and X. Tang, "Indoor non - directed optical wireless communications - Optimization of the Lambertian order," *J. Elect. Comput. Eng. Innov.*, vol. 1, no. 1, pp. 1-9, 2013.

[30] T. Komine and M. Nakagawa, "Fundamental analysis for visible-light communication system using LED lights," *IEEE Trans. Consum. Electron.*, vol. 50, no. 1, pp. 100-107, Feb. 2004.

[31] T. Komine, L. Jun Hwan, S. Haruyama, and M. Nakagawa, "Adaptive equalization system for visible light wireless communication utilizing multiple white LED lighting equipment," *IEEE Trans. on Wireless Commun.*, vol. 8, no. 6, pp. 2892-2900, June 2009.

[32] I. E. Lee, M. L. Sim, and F. W. L. Kung, "Performance enhancement of outdoor visible-light communication system using selective combining receiver," *Optoelectronics*, IET, vol. 3, pp. 30-39, 2009.

[33] Andrea Goldsmith, *Wireless Communications*, Cambridge University Press, 2005.

[34] A. J. Goldsmith and Soon-Ghee Chua, "Variable-rate variable-power MQAM for fading channels," *IEEE Trans. on Commun.*, vol. 45, no. 10, pp. 1218-1230, Oct. 1997.

[35] Von der, "Reliability Assessment of Vehicle-to-Vehicle Communication," *Thesis dissertation*, Technischen Universitt Carolo-Wilhelmina zu Braunschweig.